COMMUNICATIONS PHYSICS

ARTICLE

DOI: 10.1038/s42005-018-0075-7 OPEN

Rotating lamellipodium waves in polarizing cells

Cody Reeves[1], Benjamin Winkler[2], Falko Ziebert[3] & Igor S. Aranson[4]

Cellular protrusion- and lamellipodium waves are widespread for both non-motile and moving cells and observed for many cell types. They are involved in the cell's exploration of the substrate, its internal organization, as well as for the establishment of self-polarization prior to the onset of motion. Here we apply the recently developed phase field approach to model shape waves and their competition on the level of a whole cell, including all main physical effects (acto-myosin, cell membrane, adhesion formation and substrate deformation via traction) but ignoring specific biochemistry and regulation. We derive an analytic description of the emergence of a single wave deformation, which is of Burgers/Fisher-Kolmogorov type. Finally, we develop an amplitude equation approach to study multiple competing rotational waves and show how they allow the cell to transition from a non-moving state towards a polarized, steady moving state.

[1] Department of Engineering Sciences and Applied Mathematics, Northwestern University, Evanston, IL 60208, USA. [2] Physikalisches Institut, Albert-Ludwigs-Universität Freiburg, Hermann-Herder-Strasse 3, 79104 Freiburg, Germany. [3] Institute for Theoretical Physics, Heidelberg University, Philosophenweg 19, 69120 Heidelberg, Germany. [4] Department of Biomedical Engineering, Pennsylvania State University, University Park, Pennsylvania 16802, USA. Correspondence and requests for materials should be addressed to I.S.A. (email: isa12@psu.edu)

Animal cells adhere and move along substrates using a machinery involving the acto-myosin cytoskeleton for force generation[1–3] and adhesion protein complexes to link and transfer these forces to the substrate[4]. In many cases, spreading and motion are not monotonous processes in time but involve actin- and shape-wave phenomena[5–7]. For instance, periodic lamellipodium contraction waves have been found in adhering fibroblasts, traveling both rearwards and laterally, i.e., along the cell's periphery[8,9]. Lateral waves typically annihilate[10], hinting at excitable medium type of waves. Similar waves were also found in stationary Xenopus tissue culture cells[11]. A biological reason for the emergence of waves may be that cells try to explore the substrate to find other cells or to select an optimal environment. More recently, protrusion waves have been suggested to be also important for structuring the position of adhesion sites[12,13]. Interestingly, shape waves have also been found in *Dictyostelium discoideum*, without any contact to the substrate[14]. Finally, non-steady moving cells often display actin-related shape waves. For instance, wave generation was reported for crawling keratocyte cells[15,16] on highly adhesive substrates, where lamellipodial protrusion waves traveled at the cell's leading edge from side to side with periods of few minutes.

A second important occurrence of cellular shape waves relates to the spontaneous onset of shape polarization and directed cell migration. There, the development of a single protrusion is needed that grows and, when a sufficiently strong front–back asymmetry has been achieved, leads to persistent motion[17]. Instead of this generic scenario, the formation of multiple lamellipodia was reported[18] upon a decrease in membrane tension that apparently impedes the establishment of such a global asymmetry. Similarly, by studying keratocytes from different developmental stages of zebrafish, ref. [19] reported about cells that form several (typically 2–4) protrusions that induce an overall rotational motion of the cell, corresponding to lamellipodia running around the cell's periphery. Here the multiple protrusions are caused by regulatory processes, the rotating cell type having a higher myosin light chain kinase level, a molecule which decreases the lifetime of protrusions by increasing myosin activity. Quite similar multiple protrusion and rotating states have been also found for standard fish keratocytes directly after making first contact to the substrate when arriving from suspension[20]. There, apparently different protrusion waves are coupled and competing, with eventually one winning and taking it all and polarizing the cell.

One can argue that cell protrusion and lamellipodium waves are widespread and observed for many cell types. In contrast to actin polymerization waves that occur also in bulk[7,21–23], the coupling to both the membrane and the substrate makes the problem much richer. One-dimensional (1D) models for this phenomenon have been proposed in refs. [11,16], including several regulation steps. In two dimensions, multiple protrusions were described by a simple phenomenological model based on the cell-edge dynamics controlled by the distance from the cell center[20]. However, to date no model of lamellipodia waves exists on the level of a whole cell. Using the recently developed phase field approach, see refs. [24–36] for recent comprehensive reviews, we demonstrate the occurrence of protrusion waves and analyze their formation and competition within a minimal physical model. Our study revealed that the onset and competition of rotating lamellipodium waves can be captured in the framework of a model incorporating cell shape dynamics, actin polymerization, substrate deformation, and adhesion. Our numerical analysis of the phase field equations is supplemented by reduced models of cell membrane dynamics where qualitatively similar wave phenomena are observed. We demonstrate that the formation of rotating protrusions can be interpreted as a propagation of shock waves described by a Burgers-like equation for the position of the cell membrane. Furthermore, simple ordinary differential equations for wave competition and the onset of cell polarization can be derived, explaining why standing waves (corresponding to breathing shape modes) are ultimately unstable and how waves trigger the onset of cell polarization and motion. This work hence demonstrates that, while biochemical regulation pathways are obviously relevant to orchestrate the phenomenon and tailor it to the desired function, the emergence of waves only needs the interplay of protrusion, adhesion, and contraction. In addition to migrating cells, our findings may provide additional insights into the onset and complex shape dynamics of active droplets[37,38].

Results

Rotating lamellipodia in the computational model. The numerical results were obtained using an effectively two-dimensional (2D) model framework, whose parts have been developed previously in refs. [27–31]. Namely, the cell shape is described by a phase field $\rho(\mathbf{r}, t)$, which evaluates to 1 inside and to 0 outside with a smooth transition region in between these two states defining the membrane position. The dynamics of the actin cytoskeleton is described via a vector field $\mathbf{p}(\mathbf{r}, t)$, which has a source located at the membrane (modeling actin nucleation) and exerting forces on it (modeling actin polymerization ratcheting, parameter α) provided that adhesive bonds $A(\mathbf{r}, t)$ have been formed. Adhesive bonds follow a reaction–diffusion dynamics inside the cell and transfer pushing actin forces to the substrate via traction forces $\mathbf{T}(\mathbf{r}, t)$. The substrate is deformed (described via the displacement field $\mathbf{u}(\mathbf{r}, t)$ and Kelvin–Voigt viscoelastic response of shear modulus G), which can lead to adhesive rupture. This "feedback loop" between force exertion, transmission, and bond rupture can induce stick-slip motion, also of parts of the cell, as described previously[28,29]. Details of the model are given in the Methods section.

Although the model was originally designed to describe cell motion, Fig. 1 shows that it also captures a variety of rotational lamellipodium states. While the model is known to describe polarized, moving states—see Supplementary Movie 1—depending on parameters a cell may not be capable of polarizing, or the initial condition may not be sufficiently biased to allow for it. In both cases, transient rotational states emerge, with the cell finally settling to a non-motile circularly symmetric state in the former case or polarizing with a single lamellipodium and adopting a persistent motion in the latter. The simplest case is one rotating shape wave as demonstrated in Fig. 1a–d and Supplementary Movie 2. Multiple localized lamellipodia are also possible as demonstrated in Fig. 1e–h and Supplementary Movie 3 showing two counter-propagating shape waves and in Fig. 1i–l and Supplementary Movie 4 showing two co-propagating shape waves. Higher-order deformation modes are also observed, see Supplementary Movies 5 and 6.

Figure 2 displays the traction distribution of a polarized cell (Fig. 2a) compared to a cell displaying two counter-rotating lamellipodia (Fig. 2b) (similar to Fig. 1e–h). It is evident that both, the traction distribution and the polarization (as already shown in Fig. 1) have local maxima close to the shape deformations. Hence, they can be interpreted as local lamellipodia, similar to those occurring in the experiments[18–20].

Since the cell shape, the actin distribution, as well as the adhesion build-up and substrate deformation are all coupled, lamellipodium waves are expected to be in nonlinear competition. In fact, typically all but one wave is damped in the long term, with a dominant wave gaining in amplitude and polarizing the whole cell. For cells displaying a single shape wave, the wave travels along the cell's periphery for several turns until it eventually

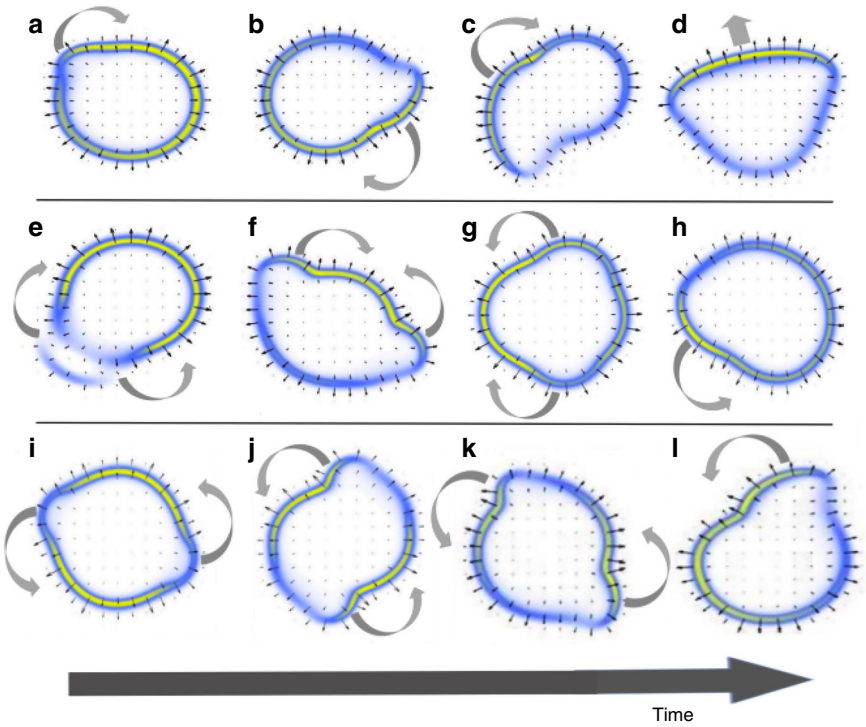

Fig. 1 Time evolution of three select rotational states. **a**–**d** shows a cell with one lamellipodium wave rotating clockwise. Finally, the cell polarizes, i.e. forms a single stable lamellipodium, leading to persistent motion. **e**–**h** shows a cell with two lamellipodium waves rotating in opposite directions. The two waves are in nonlinear competition, with one of them finally winning (**h**), again leading to polarization and persistent motion, similar to the former case. **i**–**l** shows a cell with two lamellipodium waves rotating in the the same (counterclockwise) direction. The waves exhibit similar nonlinear competition and the same long-term motility behavior as in the previous cases. The magnitude of actin polarization, **p**(**r**), is color coded (with blue for small and yellow for large values) and its direction shown as the black arrows. The gray arrows indicate the direction of rotation for the deformation waves or the direction of motion in case of a polarized cell

polarizes the whole cell. One can conclude that the wave phenomena are transient and that they finally induce directed motion. This suggests a coupling of deformation modes and the translational mode, see the discussion of wave competition below.

Figure 2c shows a phase diagram of the cellular dynamics obtained when varying the substrate stiffness G vs. the actin-associated pushing rate, α. For soft substrates, the cell polarizes immediately without noticeable initial oscillation. In turn, if the substrate is too stiff, all oscillatory modes are strongly dampened and the cell remains stationary. For slow actin dynamics, cells display a very slow, ameboid-like gliding behavior, as its effect is too weak to polarize the cell, see Supplementary Movie 7. For too high values of α, the cell is unable to maintain its integrity, with (lamellipodium) fragments beginning to split off from the main cell body. In between these boundaries in parameter space, rotational states with a diversity of modes exist: single rotating lamellipodia, double co-rotating and counter-rotating lamellipodia, and even higher modes. This corroborates that the wave phenomena emerge in the transition region between conditions where cells are easily polarizable and conditions where cells can not polarize, as an additional route to break the symmetry and initiate cell motion. Overall, the number of protrusions tends to increase with the cell's size, although the detailed dependence is not simple.

Fourier analysis of rotating states. To obtain additional insight, we extracted the Fourier modes of the cellular shape as a function of time. The position of the membrane was identified with the location of the $\rho = 1/2$-isoline. The membrane was then discretized using quadratic interpolation to produce discrete Cartesian coordinates, which were transformed into radial coordinates $(\phi, r(\phi))$ relative to the center of mass (c.o.m.) determined by $\mathbf{r}_{\mathrm{c.o.m.}} = \int \rho \mathbf{r}\, dxdy / \int \rho\, dxdy$. The Fourier modes as defined by

$$\tilde{r}_k = \sum_{n=0}^{N-1} r(\phi_n) e^{-i2\pi nk/N} \quad \text{for } k = 0, 1, 2, \ldots N-1 \qquad (1)$$

were then determined numerically performing a Fast-Fourier Transform (FFT) of $r(\phi)$.

The leading order Fourier modes are shown in Fig. 3a for the case of a single rotating wave and in Fig. 3b for the case of two counter-rotating waves. For the single wave case, the leading Fourier modes monotonically increase until the rotating wave is strong enough to polarize the cell. For the two wave case, the plot shows a periodic pattern—as the two waves separate on one side of the cell and collide on the opposite side. Eventually, one wave wins the competition, the weaker becomes damped and from this point on the Fourier modes resemble the single wave case. In the process of polarization, the cell typically forms a transient elongated elliptical shape, as demonstrated in Fig. 1c. Finally, it eventually stabilizes into the steady gliding shape, as seen in Fig. 1d. The build-up of this transient elongated shape is why the second mode dominates the Fourier spectrum prior to cell polarization.

In the following, we will investigate in more detail the formation of the waves, how these waves interact and compete with each other, and how the rotational states eventually polarize the cell.

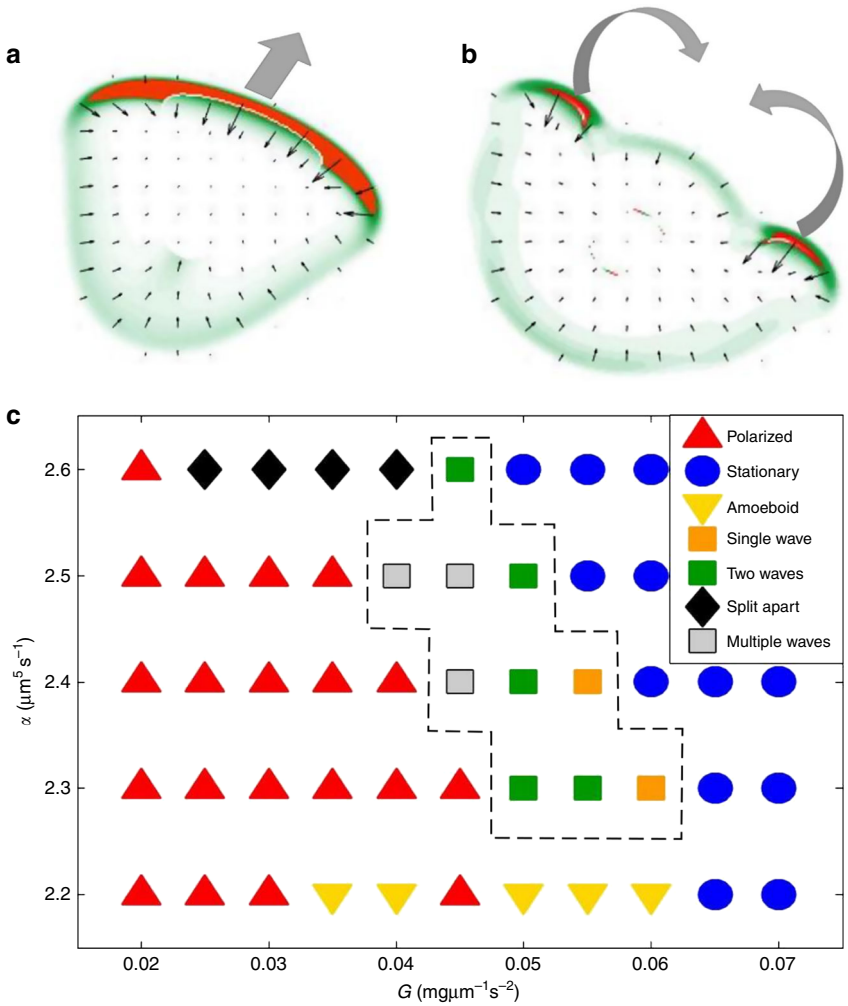

Fig. 2 Traction distribution and diagram of cellular states. Shown is the distribution of traction forces, **T**(**r**), for a polarized cell (**a**) and for a cell with two counter-rotating lamellipodia (**b**). The magnitude of the traction force is color coded (green for small and red for large values) and its direction given by black arrows. Gray arrows indicate directed motion or rotation, respectively. **c** Phase diagram of the different types of cellular dynamics in the plane actin pushing rate α vs. substrate stiffness G. The area enclosed in dashed lines (guide to the eye) is the region where rotational waves are observed

Formation of rotational waves. To understand the formation process of localized lamellipodium waves, we performed an asymptotic reduction of the full computational model. We approximate the phase field for a quasi-circular cell close to the stationary state as

$$\rho(r,\phi,t) = \frac{1}{2}\left[1 - \tanh\left(\frac{r - r_0(\phi,t)}{2\sqrt{2D_\rho}}\right)\right], \qquad (2)$$

where $r_0(\phi, t)$ is the location of the cell membrane, see also ref. [39]. As shown in Methods, we can approximate the stationary values of the adhesion field and the actin polarization close to the cell's boundary by $A_s \approx a_{nl}\rho/s$, and $\mathbf{p}_s \approx -\beta\nabla\rho/\left[\tau_1^{-1} + (3/4)\tau_2^{-1}\right]$. Using these approximations, the dynamic phase field equation can then be reduced by evaluating the corresponding solvability condition to a single 1D partial differential equation for the membrane deformation, δr_0, from a reference value R_0, i.e., $\delta r_0(\phi, t) = r_0(\phi, t) - R_0$:

$$\begin{aligned}\partial_t(\delta r_0) = {} & \tfrac{D_\rho}{R_0^2}\partial_\phi^2(\delta r_0) - \sqrt{2D_\rho}\mu\delta V \\ & - \tfrac{D_\rho}{R_0}\left(1 - \tfrac{\delta r_0}{R_0}\right) + \tilde{\alpha} + \tfrac{\tilde{\alpha}}{R_0^2}\left(\partial_\phi(\delta r_0)\right)^2,\end{aligned} \qquad (3)$$

where $\delta V = \frac{1}{2}\int_0^{2\pi}(\delta r_0 + R_0)^2 d\phi - \pi R_0^2$ is related to the volume conservation of the cell (corresponding in the effective 2D model to the conservation of the cell's contact area). $\tilde{\alpha}$ is an effective parameter containing the actin polymerization rate, the pushing force it exerts, and the myosin-mediated contractile forces in a combined fashion (see Methods, Eq. (27), and subsequent discussion). The equation has a diffusive term and a contribution from volume conservation. The third term leads to linear growth of perturbations, while the nonlinear term $\sim(\partial_\phi\delta r_0)^2$ saturates the growth. Finally, the pushing due to actin polymerization leads to a source term attempting to globally increase δr_0.

This Burgers-like equation suggests that the lamellipodium waves are a kind of shock wave traveling around the cell's periphery as the result of some small local perturbation in δr_0. In fact, a numerical integration of Eq. (3), using as initial condition a small narrow peak, is shown in Fig. 4a and Supplementary Movie 8: two rotating waves develop and travel in opposite directions; the front of the wave is where $|\partial_\phi\delta r_0|$ is the largest. The diffusion term diminishes the back end of the wave, while δV ensures the conservation of the overall volume of the cell. The qualitative behavior is the same as for the full phase field model shown in Fig. 4b, where the cell radius r_0 was interpolated from a simulation, see the Fourier analysis of rotating states discussed above.

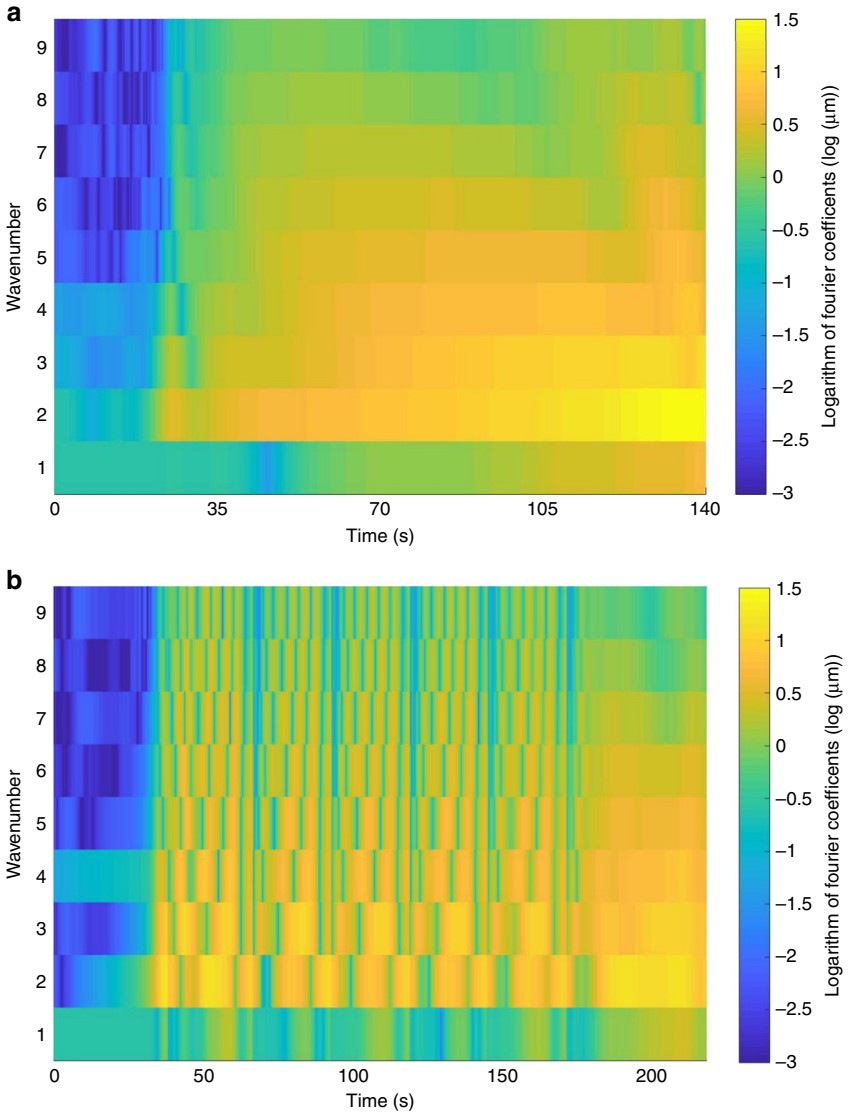

Fig. 3 Time evolution of the amplitudes (in logarithmic scale) of the leading Fourier modes of the cellular shape. **a** A single rotating wave and **b** two competing counter-rotating waves, with finally one of them winning

The deformation dynamics of lamellipodia is caused by the simultaneous action of molecular motors and the ratcheting of actin, pushing the membrane out radially in a, in general, non-uniform fashion. This is countered by a restoring force resulting from the conservation of area. Since actin is oriented roughly normal to the membrane, once a lamellipodium protrusion forms the actin along the sides of the lamellipodium has a significant component in the azimuthal direction. This effect is present in Eq. (3) as the last term as $|\partial_\phi(\delta r_0)|$ is greatest along the lamellipodium sides. The azimuthal component then forces the lamellipodium to begin rotating with the lamellipodium sides becoming the wave fronts: the actin along one side forces it clockwise and the other counterclockwise, effectively splitting the protrusion into two separate counter-rotating waves. The most generic scenario observed is hence a pair of counter-rotating waves originating from a single lamellipodium.

By applying a Cole–Hopf transformation, $\delta r_0 = (D_\rho/\tilde{\alpha})\log(W)$, the Burgers-like Eq. (3) can be reduced to a Fisher–Kolmogorov–Petrovsky–Piskunov-type equation[40]

$$\partial_t W = \frac{D_\rho}{R_0^2}\partial_\phi^2 W - \frac{\tilde{\alpha}}{R_0} W\left(1 + \widetilde{\delta V} - \frac{D_\rho}{\tilde{\alpha} R_0}\log(W)\right), \qquad (4)$$

where $\widetilde{\delta V} = \frac{R_0}{\tilde{\alpha}}(\sqrt{2D_\rho}\mu\delta V - \tilde{\alpha})$. From its structure, this equation is known to allow for moving fronts connecting stable and unstable equilibria in certain parameter regimes. Further analysis of this equation is detailed in Methods. Especially, the existence of transient traveling wave solutions around $r_0 \simeq R_0$ is found by phase plane analysis, supporting the numerical findings.

Competition of rotational waves. While the previous section explains the formation of the rotating waves, the question remains how different rotational modes are coupled together, as well as how the waves affect the cell's velocity and vice versa. We here propose a phenomenological dimensionless reduced system of ordinary differential equations to explain the dynamics of wave competition, as well as how waves trigger cell polarization.

For simplicity, consider two rotating waves with complex amplitudes R_1 and R_2, each with corresponding frequency ω_1 and ω_2. The waves are assumed to be small perturbations of the circular cell, i.e., $r_0(\phi, t) = R_0[1 + R_1(\phi, t)\exp(i\omega_1 t) + R_2(\phi, t)\exp(i\omega_2 t)] + \text{c.c.}$, such that $|R_1|, |R_2| \ll 1$. Then, as detailed in Methods, a system of amplitude equations can be derived by

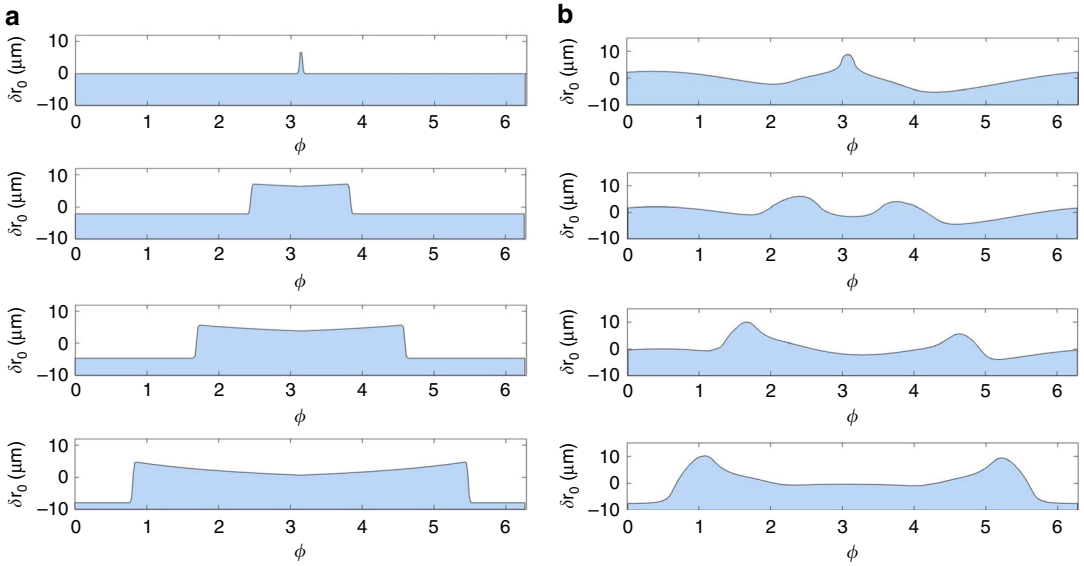

Fig. 4 Propagation of a pair of shape waves. **a** Time evolution of the perturbation of the cell radius $\delta r_0(\phi)$ vs. ϕ using the asymptotic reduced description, Eq. (3). **b** Time evolution obtained from the full phase field model. The initial condition for **a** was a narrow symmetric perturbation on an otherwise circular cell. Both pictures clearly show the emergence of a pair of waves moving in opposite directions

evaluating the solvability condition of the system:

$$\partial_t R_1 = \epsilon R_1 - \zeta\left(|R_1|^2 + \gamma|R_2|^2\right)R_1, \tag{5}$$

$$\partial_t R_2 = \epsilon R_2 - \zeta\left(|R_2|^2 + \gamma|R_1|^2\right)R_2. \tag{6}$$

Here ϵ is the supercriticality parameter, ζ describes amplitude saturation, and γ is the wave coupling parameter. For $\gamma > 1$, only one wave survives competition, the surviving wave being determined by the initial conditions. As we obtain $\gamma = 2$ (see Methods), this is indeed the case for the system at hand, explaining the behavior observed in Fig. 3b). As shown in the Methods section, the supercriticality parameter ϵ is proportional to the (square of the) actin polymerization parameter β of the phase field model: in fact, actin pushes the membrane outwards radially and causes the waves to grow in size. The amplitude saturation parameter ζ in turn is proportional to the parameter d_0 in the underlying model, which describes the rupturing of adhesions due to high cell traction: the higher the rupturing rate, the lower the force that can be transferred and consequently the lower the protrusion force and the size of the protrusion. Note that this parameter was not significant for the formation of the waves, but it is for the competition of multiple waves.

Now let us consider the time evolution for the cell's center of mass velocity. It is convenient to formally rewrite the velocity vector, $\mathbf{v} = v_x\hat{x} + v_y\hat{y}$, as a "complex velocity," $\hat{V} = v_x + iv_y$. First, we take the velocity to be uncoupled to the rotating waves. Motivated by the observation that in the full model cells exhibit a subcritical transition to the moving state[27,28], we suggest the following generic equation for the onset

$$\partial_t \hat{V} = g\left(\hat{V}\right) = -a\hat{V} + b\left|\hat{V}\right|^2 - c\left|\hat{V}\right|^4\hat{V}. \tag{7}$$

In fact, this equation has a subcritical transition toward motion, if a, b, $c > 0$ and $(b/c)^2 - 4a/c > 0$. In this case, there are three equilibria: $V_0 = 0$ and

$$V_\pm^2 = b/2c \pm \sqrt{(b/2c)^2 - a/c}. \tag{8}$$

Both V_0 (stationary cell) and V_+ (polarized cell) are stable, while V_- is an unstable solution.

Now, the symmetry—i.e., the fact that the translation mode has the angular dependence $\exp(i\phi)$—suggests the following leading order coupling of the center of mass velocity and the rotational waves

$$\partial_t \hat{V} = g\left(\hat{V}\right) + q_1\left(R_1 e^{i\omega_1 t} + R_2 e^{i\omega_2 t}\right) + q_2\left(|R_1|^2 + |R_2|^2\right)\hat{V}, \tag{9}$$

$$\partial_t R_1 = \epsilon R_1 - \zeta\left(|R_1|^2 + \gamma|R_2|^2 + w\left|\hat{V}\right|^2\right)R_1, \tag{10}$$

$$\partial_t R_2 = \epsilon R_2 - \zeta\left(|R_2|^2 + \gamma|R_1|^2 + w\left|\hat{V}\right|^2\right)R_2. \tag{11}$$

For our sakes, we are only concerned with the real components of the rotating waves. Results from Eqs. (9)–(11) can also be compared to simulations using the full computational model in a similar fashion as described above for the Fourier mode analysis: we interpolated r_0 and determined the location of the peak of the jth wave in polar coordinates (r_j, ϕ_j). Its amplitude can then be evaluated as $R_j = \exp(i\phi_j)(r_j - R_0)/R_0$. Finally, the cell's center of mass velocity can be evaluated by taking the time derivative of the center of mass position, $\mathbf{v} = \dot{\mathbf{r}}_{\text{c.o.m.}}$.

Let us first consider the case of one wave rotating with frequency $\omega_1 = \omega$. As shown in Fig. 5a as the solid curves, the rotating wave perturbs the cell, inducing oscillations of the cell's center of mass velocity, as seen in the terms $\propto q_1$, q_2 in Eq. (9). Eventually, the velocity stabilizes to V_+ since, in turn, it dampens the rotating wave as expressed by the terms $\propto w$ in Eqs. (10) and (11). In the full computational model, the dashed curves, the cell has a transient elongated elliptical shape when it polarizes, accompanied by an increasing velocity, and the cell eventually settles in the steady moving state. We can also consider the case of two counter-rotating waves such that $\omega_1 = -\omega_2 = \omega$, as shown in Fig. 5b. Qualitatively, the counter-rotating case is similar to the single wave case: as before, the rotating waves disturb the cell causing oscillations in the velocity. The two waves compete until only one survives and the other is damped, with the initial conditions determining which one of the waves survives. Eventually, the cell polarizes and its velocity dampens the last remaining rotating wave (blue curve). Figure 5a, b directly compare the dynamics of the reduced amplitude equations to the

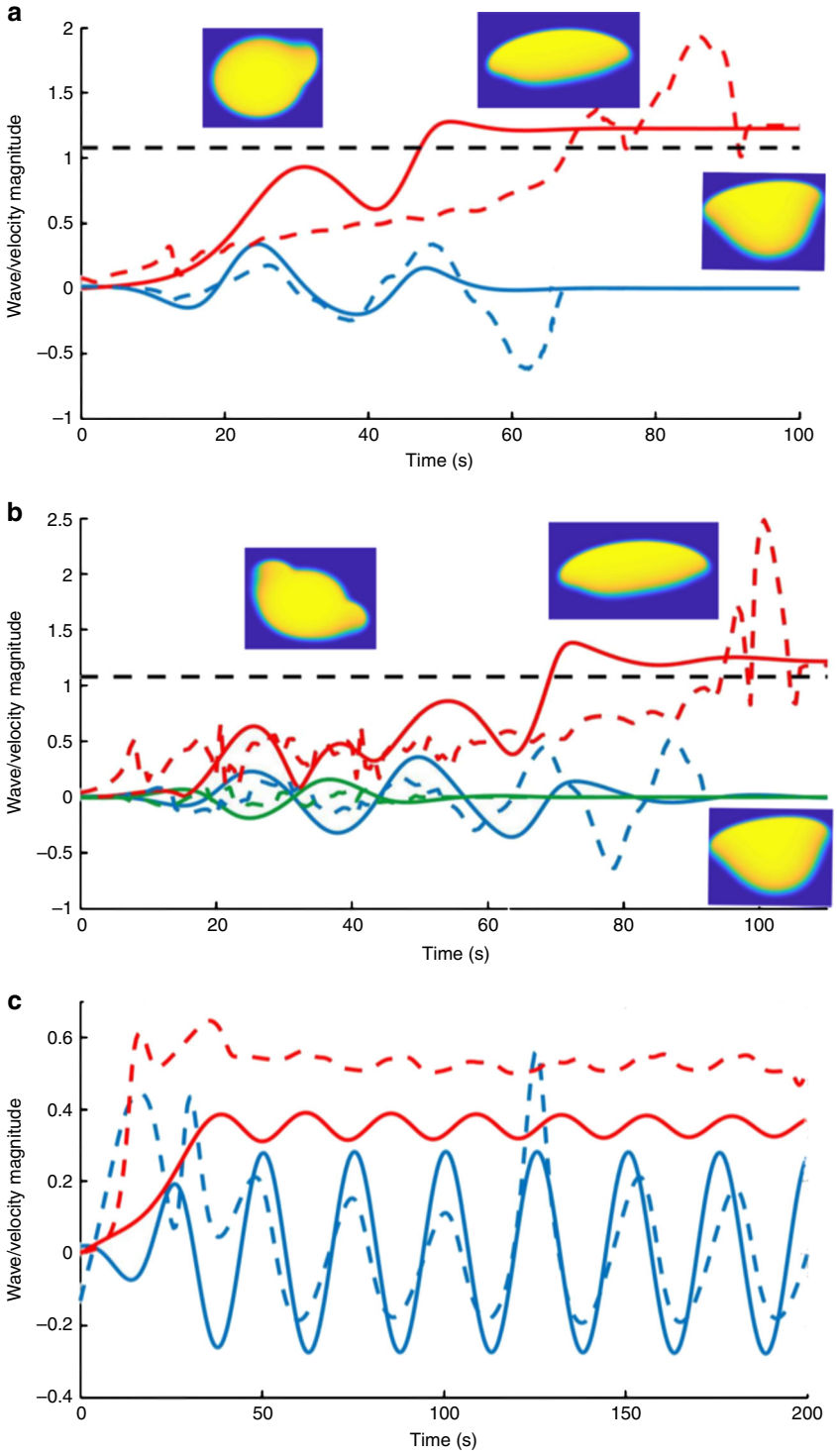

Fig. 5 Coupling of rotating waves and center of mass motion. **a**–**c** Shown are the real components of rotating waves, R_1 (in blue) and R_2 (in green, if applicable), and the center of mass velocity of the cell (in red) for different scenarios: **a** a single rotating wave, **b** two waves rotating in opposite directions with the same angular frequency, **c** a single wave that is less driven by the actin-related processes (i.e., with smaller ϵ). In **a**–**c**, continuous curves have been obtained using the reduced amplitude Eqs. (9)-(11), the dashed curves using the full phase field model (with insets corresponding to the respective shapes). The velocity from the full phase model has been rescaled for viewing purposes and the reduced amplitude equations are non-dimensionalized. The black horizontal dashed line indicates the unstable velocity V_-. The timescale for the full model was normalized to the timescale of the reduced model. For **c**, the R_1 values from the full model were taken to be the second moment of ρ and the amplitude was normalized for comparison. Parameters for the reduced model: $\omega = 0.25$, $\gamma = 2.0$, $\zeta = 1.0$, $w = 0.18$, $a = 0.12$, $b = 0.23$, $c = 0.1$, $q_1 = 0.3$, $q_2 = 0.7$; $\epsilon = 0.2$ for **a**, **b** and $\epsilon = 0.1$ for **c**

one obtained in the full phase field model (solid vs. dashed curves). Although the oscillations differ in amplitude and are more complex in the full model—due to the neglect of higher modes in the reduced model—the general behavior is well captured.

Finally, we can consider the case of a single rotating wave with $\omega_1 = \omega$ and using a smaller ϵ value. This case provides insight into the ameboid-like motility as found in Fig. 2b. Note that this motility state is common for low values of α (one has $\epsilon \propto \alpha^2$ as we used $\beta \propto \alpha$, see Methods and Supplementary Table 1). Often the oscillations for this state are not distinct rotating waves about a roughly circular cell but instead cause shape deformations of the whole cell. It is then instructive to measure the strength of the oscillation by tracing the second moment of ρ with respect to the center of mass: $\int (\mathbf{r} - \mathbf{r}_{\mathrm{c.o.m.}})^2 \rho(x,y) dxdy$. In this case, the rotational oscillation is not capable to drive the cell's velocity beyond the unstable node (V_-). Instead, eventually both the center of mass velocity and the shape wave coexist and oscillate out of phase with respect to each other, as seen in Fig. 5c. Therefore, a possible explanation for the ameboid-like motion is that weak rotational oscillations continue to exist, forcing the cell to periodically change speed and direction, similar to the meandering core of a spiral wave[41].

Discussion

We used a whole-cell model that incorporates all relevant physical processes—the dynamics of the actin-myosin network, the formation of adhesive bonds to the substrate, and the substrate deformation via cellular traction forces—to study shape waves of spreading and polarizing cells. Although we neglected the specific biochemistry and regulation pathways present within the cell, rotating lamellipodium waves similar to those seen experimentally have been found and we could investigate in depth their occurrence, their competition, and their triggering of directed motion.

Our study suggests that the rotating states occur only within a limited range of the parameters—as exemplified by the actin propulsion rate and the substrate stiffness—and that the emergence of these waves enlarges the parameter range wherein cells are able to polarize. It also shows that the emergence of these waves only requires protrusion, adhesion, and feedback via traction-mediated breaking of adhesive bonds. One can anticipate a roughly linear increase in the number of protrusions with an increase in cell size. However, owing to nonlinear interaction between the protrusion waves, the cell size dependence is more complex and requires an in-depth computational study, which is beyond the scope of this work.

Our analysis is presently limited to a 2D description. This approximation is justified by the fact that the lamellipodium thickness is much smaller than the spatial scale of the protrusions and that the cell body is typically not participating in the front dynamics. One may hence expect that a three-dimensional consideration of the phenomenon will not change the qualitative conclusions on the physical mechanisms associated with rotating lamellipodia waves. A delicate point, however, is to what extent the spreaded area is conserved or changed by material flow from the third dimension. Hence, a 3D analysis may bring additional insights into the spatial and temporal organization of lamellipodium waves but at this point is still computationally prohibitive and left for future study.

Another important question is to what extent external stimuli and/or internal regulation processes lead to similar shape waves and rotating states or whether they only orchestrate the ones induced by the described physical mechanism. To answer this question, as demonstrated in ref. [42], the approach can be generalized to account for the currently discussed regulation pathways, like Rho/Rac guanosine triphosphate (GTP)-ases[43] or Ena/VASP proteins[16].

The developed analytical reduced description for how perturbations in the cell's periphery lead to the formation of rotating waves will stimulate further analysis. Not only is its agreement with the full numerics very reasonable but, importantly, such equations of Burgers- or Fisher–Kolmogorov–Petrovsky–Piskunov-type, respectively, put the cellular shape waves in the mathematically well-studied framework[44] of waves in reaction–diffusion systems or excitable media and allow future analytical in-depth studies.

Finally, the proposed amplitude equations allowed us to rationalize competition of cellular shape waves and on a phenomenological level also how these waves can trigger—via generic symmetry-imposed couplings—the onset of the cell's center of mass velocity. This framework is again capable of reproducing the dynamics seen in the full cell model semi-quantitatively. It may also provide insight into the onset of rotating states in related systems like active droplets[45] and the so-called "circus movements"[46,47] found in blebbing blastomere cells from, e.g., fish embryos, where single blebs travel around the cell's periphery for long times.

While the present work focused on the dendritic actin near the membrane, future work could also incorporate actin waves experimentally seen in the bulk of the cell[21,23] and study how they induce and/or affect rotational states. Furthermore, similar concepts and ideas can be used for the description of active poroelastic droplets modeling *Physarum polycephalum* dynamics[48,49]. Another intriguing aspect is the possibility of synchronization of shape waves of different, close-by cells due to mechanical and chemical interactions, calling for dedicated experiments.

Methods

Model. As developed in refs. [27,29,31], we use the following fields to describe effectively the 2D cell: first, an Allen–Cahn phase field, with $\rho(\mathbf{r}, t) = 1$ inside the cell and $\rho = 0$ outside, augmented by a (2D) volume conservation to model the cell shape; second, a vector field $\mathbf{p}(\mathbf{r}, t)$ describing the actin orientation and degree of ordering. And third the density of engaged adhesive bonds $A(\mathbf{r}, t)$ that is coupled to the deformable substrate.

The phase field equation reads

$$\partial_t \rho = D_\rho \Delta \rho - (1-\rho)\big(\delta(\rho) - \sigma|\mathbf{p}|^2 - \rho\big)\rho - \alpha A(\mathbf{p}\cdot\nabla\rho) \tag{12}$$

with the phase field parameter given by

$$\delta(\rho) = \frac{1}{2} + \mu\left[\int \rho dxdy - \pi R_0^2\right]. \tag{13}$$

Here $\delta = \frac{1}{2}$ is the stationary point and the second term introduces 2D contact area conservation with target area $V_0 = \pi R_0^2$ for some fixed radius R_0, with the stiffness of the constraint given by μ. As explained in more detail before[27], the term $\propto\sigma$ models actin network contraction by myosin molecular motors with constant rate σ and the last term models the motion ("advection") of the membrane due to the ratcheting of actin filament polymerization, with velocity α. Only adhering filaments can transfer the force to the substrate, hence the proportionality to A.

The equation modeling actin dynamics reads

$$\partial_t \mathbf{p} = D_p \Delta \mathbf{p} - \beta e^{-T_1 c \delta S} \nabla\rho - \tau_1^{-1}\mathbf{p} - \tau_2^{-1}(1-\rho^2)\mathbf{p} - \gamma(\nabla\rho\cdot\mathbf{p})\mathbf{p}. \tag{14}$$

The first term accounts for diffusion of actin filaments/elasticity in the ordered state. The second term is a source and models that actin is generated at the membrane with (polymerization) rate β. It includes the effect of membrane tension feedback on polymerization as developed in ref. [31]: The constant T_1 sets the strength of the membrane tension, $c = -\nabla\cdot\frac{\nabla\rho}{|\nabla\rho|}$ is the local curvature of the cell membrane and $\delta S = \frac{S(\rho)-S_0}{S_0}$ is (proportional to) the excess surface area, where $S(\rho) = \int|\nabla\rho| dxdy$ and $S_0 = 2\pi R_0 + 4\pi\sqrt{2D_\rho}\log 2$ are, respectively, the instantaneous and the reference surface area, the latter being defined as $S(\rho_s)$ with ρ_s from Eq. (19) below. The next two terms in Eq. (14) are sinks and model the degradation/depolymerization of actin filaments inside the cell with the typical timescale τ_1 and suppress actin outside the cell, respectively. The final term coarsely models the myosin motors' ability to form antiparallel actin bundles reducing the actin polarization and breaks the symmetry between the front and rear of the cell[27].

The engaged adhesion bonds are modeled by an equation of reaction–diffusion type as

$$\partial_t A = D_A \Delta A + \rho\left(a_0|\mathbf{p}|^2 + a_{nl}A^2\right) - \left(d(u) + sA^2\right)A. \quad (15)$$

The first term is diffusion and the second term models attachment, a linear contribution in the presence of actin, and a nonlinear one modeling collective effects. The third term restricts the amount of adhesions by excluded volume, $\propto s$, and substrate-dependent detachment. The detachment rate

$$d(u) = \frac{d_0}{2}\left[1 + \tanh\left(b\left(|\mathbf{u}_{z=H}|^2 - u_c^2\right)\right)\right] \quad (16)$$

accounts for the fact that the substrate is soft and deformed by the cell via the traction forces it exerts on it. In Eq. (16), we made the assumption that adhesions will break where the local substrate deformation directly underneath the cell, $|\mathbf{u}_{z=H}| = |\mathbf{u}(x, y, z = H)|$, exceeds a critical value u_c. The substrate is modeled as a 3D isotropic homogeneous visco-elastic solid of Kelvin–Voigt type, introducing the shear modulus G, a viscosity η (modeling viscous losses due to adhesion rupture), and the effective height of the substrate, H. This treatment has been thoroughly discussed in refs. [29,36], yielding the displacement at the top of the substrate, $\mathbf{u}_{z=H}$, due to the traction force distribution exerted by the cell, defined as

$$\mathbf{T} = -A\rho\left(\mathbf{p} + cT_1\delta S\hat{n} - \frac{\int A(\mathbf{p} + cT_1\delta S\hat{n})\rho\, dxdy}{\int A\rho\, dxdy}\right). \quad (17)$$

Here the first two terms in the bracket are the counter forces related to actin polymerization and membrane tension preserving the membrane surface area. The final term is of frictional origin and ensures that the net force on the substrate is zero, as it should, the cell being an isolated self-propelled object.

Numerical method. The system of equations Eqs. (12), (14), and (15), including the displacement field $\mathbf{u}_{z=H}$, were solved numerically using a highly parallelized algorithm implemented on a graphics processing unit, using Compute Unified Device Architecture (CUDA). As the phase field takes care of the deformable and/or moving boundaries, the problem can be solved on a double periodic square domain using classical operator splitting[50], pseudo-spectral method, and FFT. For a more comprehensive review of the numerical scheme, see ref. [36]. The phase field curvature was computed (using finite differences) only in a tube around the cell membrane[31]. Typical parameter values are listed in Supplementary Table 1. Field distributions for a stationary cell are shown Supplementary Fig. 1.

The qualitative motility behavior was tested to be consistent when refining the spatial mesh or the time step. Simulations were started with a small amount of random noise added within the circular region modeling the cell, where the initial value of the phase field is $\rho(x, y, t = 0) = 1$. The polarization of the cell and/or the formation of rotating waves was consistent irregardless of the initial noise; the noise realization, however, affects the direction of polarization or, in the case of multiple waves, which wave dominates and survives.

Derivation of reduced descriptions of wave formation. Consider first the homogenous 1D case of the phase field equation. Rewriting it as $\partial_t\rho = \mathcal{L}_\rho[\rho]$ using the self-adjoint differential operator $\mathcal{L}_\rho$

$$\mathcal{L}_\rho[\rho] = D_\rho\delta_r^2\rho - (1-\rho)(1/2-\rho)\rho, \quad (18)$$

it is easy to show that

$$\rho_s(r) = \frac{1}{2}\left[1 - \tanh\left(\frac{r - R_0}{2\sqrt{2D_\rho}}\right)\right] \quad (19)$$

is the solution of $\mathcal{L}_\rho[\rho_s] = 0$, i.e., ρ_s solves the stationary 1D phase field equation [for ease of notation, one defines $\tilde{r} = (r - R_0)/(2\sqrt{2D_\rho})$]. If we assume a large cell $(R_0/\sqrt{D_\rho} \gg 1)$, it can be also shown that Eq. (19) is the leading order approximation for the stationary solution of the 2D homogeneous phase field equation.

Now consider the full system of equations. For simplicity, we will ignore the diffusion terms of $\mathbf{p}$ and A, take $\delta S = 0$, and define $\delta V = \int \rho dxdy - \pi R_0^2$:

$$\partial_t\rho = D_\rho\Delta\rho - (1-\rho)\left(\frac{1}{2} - \mu\delta V - \sigma|\mathbf{p}|^2 - \rho\right)\rho - \alpha A(\mathbf{p}\cdot\nabla\rho) \quad (20)$$

$$\partial_t\mathbf{p} = -\beta\nabla\rho - \tau_1^{-1}\mathbf{p} - \tau_2^{-1}(1-\rho^2)\mathbf{p} - \gamma(\nabla\rho\cdot\mathbf{p})\mathbf{p} \quad (21)$$

$$\partial_t A = a_0\rho|\mathbf{p}|^2 + a_{nl}\rho A^2 - sA^3 - d(u)A \quad (22)$$

We assume that the terms involving $d(u)$ and a_0 in the adhesion equation are negligible for the stationary case; we will include and discuss them later. Therefore, we can approximate the stationary solution as $A_s \approx \frac{a_{nl}}{s}\rho$. For the region inside the cell ($\rho = 1$), the stationary values then are $\mathbf{p}_s = 0$ and $A_s \approx a_{nl}/s$, while outside the cell ($\rho = 0$) one trivially has $\mathbf{p}_s = 0$ and $A_s = 0$.

The actual region of interest is the one near the cell membrane ($|\tilde{r}| \ll 1$). Expanding Eq. (19), one gets the stationary values in this region as $\rho_s \approx 1/2$ and hence $A_s \approx \frac{a_{nl}}{2s}$. Furthermore, we can approximate $\mathbf{p}_s$ by setting $\partial_t\mathbf{p}_s = 0$ and taking the scalar product of Eq. (21) with $\nabla\rho$ to obtain

$$0 = -\beta|\nabla\rho|^2 - \left(\tau_1^{-1} + (3/4)\tau_2^{-1}\right)(\mathbf{p}_s\cdot\nabla\rho) - \gamma(\mathbf{p}_s\cdot\nabla\rho)^2, \quad (23)$$

which can be solved to get approximately

$$\mathbf{p}_s \approx \frac{-\beta}{\tau_1^{-1} + (3/4)\tau_2^{-1}}\nabla\rho = -\tilde{\beta}\nabla\rho, \quad (24)$$

defining $\tilde{\beta}$ as the effective polymerization vs. degradation rate of the actin filaments. These approximations for the stationary values of ρ, A, and $\mathbf{p}$ are compared to the numerically obtained values in the full model in Supplementary Fig. 2.

We now generalize Eq. (19) to non-circular cells with radius $r_0(\phi, t)$, as already given in Eq. (2). Assuming small perturbations of the stationary state, we can use $A \approx A_s$ and $\mathbf{p} \approx \mathbf{p}_s$ and write Eq. (20) as $\mathcal{L}_\rho[\rho] = 0$ with

$$\begin{aligned}\mathcal{L}_\rho[\rho] = \partial_t\rho - \tfrac{D_\rho}{r}\partial_r\rho - \tfrac{D_\rho}{r^2}\partial_\phi^2\rho + \mu\delta V(1-\rho)\rho \\ -\sigma\tilde{\beta}^2\rho(1-\rho)|\nabla\rho|^2 - \tfrac{\alpha a_{nl}\tilde{\beta}}{s}\rho|\nabla\rho|^2.\end{aligned} \quad (25)$$

Now, in order for a nontrivial solution of Eq. (25) to exist, its solvability condition $\langle\partial_r\rho, \mathcal{L}_\rho[\rho]\rangle = 0$ must be satisfied, where the inner product is defined by $\langle A, B\rangle = \int_0^{2\pi}\int_0^\infty AB r dr d\phi$ and $\partial_r\rho$ is the solution to the linearized Eq. (20). In the large cell limit and using Eq. (2), a straightforward calculation shows that the solvability condition is satisfied given the following equation is fulfilled

$$\partial_t r_0 = \frac{D_\rho}{r_0^2}\partial_\phi^2 r_0 - \left(\mu\sqrt{2D_\rho}(\delta V) - \tilde{\alpha}\right) - \frac{D_\rho}{r_0} + \tilde{\alpha}\left(\frac{\partial_\phi r_0}{r_0}\right)^2, \quad (26)$$

with the effective actin propulsion parameter

$$\tilde{\alpha} = \frac{\tilde{\beta}}{10\sqrt{2D_\rho}}\left(\frac{\alpha a_{nl}}{s} + \frac{3\sigma\tilde{\beta}}{7}\right). \quad (27)$$

Note that this parameter contains all main non-equilibrium effects of the cytoskeleton: polymerization vs. degradation ($\tilde{\beta}$), actin ratcheting, and force generation against the membrane (α) provided actin adheres (a_{nl}), as well as acto-myosin contraction (σ). Finally, introducing $\delta r_0(\phi) = r_0(\phi) - R_0$ as the radial perturbation from R_0, Eq. (26) can be rewritten in the form given by Eq. (3).

This Burgers-like equation can be transformed into the Kolmogorov-type Eq. (4) as indicated in the main text.

Studying traveling waves, by assuming $W(\phi, t) = Z(\phi - \omega t) = Z(\xi)$, this equation further simplifies into a second-order differential equation (ODE), and finally, introducing $Y = \partial_\xi Z$, into a system of first-ODEs

$$\partial_\xi Z = Y,\ \partial_\xi Y = -\omega\frac{R_0^2}{D_\rho}Y + \frac{\tilde{\alpha}}{R_0}Z\left(1 + \widetilde{\delta V} - \frac{D_\rho}{\tilde{\alpha}R_0}\log(Z)\right). \quad (28)$$

Using linear stability analysis and assuming $\widetilde{\delta V} \approx 0$, the system has a saddle point at $(Z, Y) = (0, 0)$ and a stable node at $(Z, Y) = (\exp(\tilde{\alpha}R_0/D_\rho), 0)$, corresponding to large shape deformations ($\delta r_0 \simeq R_0$). The phase plane flow of Eq. (28) is shown in Supplementary Fig. 2.

Derivation of equations describing wave competition. Having demonstrated that rotating waves can form from a perturbed circular cell, we now assume their existence and deduce equations for how the amplitudes of several waves as well as the cell's center of mass velocity couple. In order to do so, we include the terms of the adhesion Eq. (15) that were previously neglected (but still neglect diffusion). Similar to the previous section, we define

$$\mathcal{L}_A[A] = -a_{nl}\rho A^2 + sA^3 \quad (29)$$

and accordingly write Eq. (22) as

$$\mathcal{L}_A[A] = \partial_t A - a_0\rho|\mathbf{p}|^2 + d(u)A. \quad (30)$$

Taking the previously obtained result, $A_s = \frac{a_{nl}}{s}\rho$, we know that it fulfills $\mathcal{L}_A[A_s] = 0$.

Now we consider a cell with two harmonic rotating waves, with small non-dimensional amplitude R_i and angular frequency ω_i. We can hence write the cell's radius r_0 as

$$r_0(\phi, t) = R_0\left[1 + R_1(\phi, t)e^{-i\omega_1 t} + R_2(\phi, t)e^{-i\omega_2 t}\right] + \text{c.c.}, \quad (31)$$

with $|R_1|, |R_2| \ll 1$. Furthermore, we will assume $A(r, \phi, t) \approx \frac{a_{nl}}{s}\rho(r, \phi, t)$ and $\mathbf{p}(r, \phi, t) \approx -\tilde{\beta}\nabla\rho(r, \phi, t)$, with ρ given by Eq. (2).

The step-like detachment of adhesive bonds, $d(u)$, as defined in Eq. (16) and entering Eq. (30) is triggered by an increase of substrate deformation, $|\mathbf{u}_{z=H}|^2$, caused in turn by the traction force exerted by the cell. As evident from Fig. 1a,

the traction distribution is significant primarily at the front of the traveling waves. This can also be seen by explicitly evaluating $|\mathbf{T}|^2 \approx |-\rho A p|^2$ using the approximations listed above,

$$|\mathbf{T}|^2 \approx \left(\frac{a_{nl}\tilde{\beta}}{4s\sqrt{2D_\rho}}\right)^2 \mathrm{sech}^4\left(\frac{r-r_0}{2\sqrt{2D_\rho}}\right)\left[1+\left(\frac{\partial_\phi r_0}{r}\right)^2\right] \tag{32}$$

showing that the traction is high, due the perturbations of the cell's radius r_0, only near the front where actin polarization is high. We can therefore approximate Eq. (16) by $d(u) \approx d_0|\partial_\varphi r_0|^2|\nabla\rho|$, which, as we assume harmonic traveling waves and extract only slowly-varying contribution, further simplifies to

$$\begin{aligned} d(u) \approx\ & d_0|R_1 e^{-i\omega_1 t} + R_2 e^{-i\omega_2 t}|^2|\nabla\rho| \\ & d_0\left(|R_1|^2+|R_2|^2+R_1R_2^* e^{i(\omega_2-\omega_1)t} + R_1^*R_2 e^{i(\omega_1-\omega_2)t}\right)|\nabla\rho| \end{aligned} \tag{33}$$

where R_i^* denotes the complex conjugate of R_i.

Using all the approximations motivated above, Eq. (30) reads

$$0 = \mathcal{L}_A\left[\frac{a_{nl}}{s}\rho\right] = \frac{a_{nl}}{s}\partial_t\rho - a_0\tilde{\beta}^2|\nabla\rho|^2\rho + d(u)\frac{a_{nl}}{s}\rho \tag{34}$$

and integration yields the condition

$$0 = \int_0^{2\pi}\int_0^{\infty}\left[\frac{a_{nl}}{s}\partial_t\rho - a_0\tilde{\beta}^2|\nabla\rho|^2\rho + d(u)\frac{a_{nl}}{s}\rho\right] r dr d\phi. \tag{35}$$

It is then straightforward to show, using Eqs. (2), (31), and (33), that Eq. (35) is satisfied if the amplitudes R_1 and R_2 follow the coupled amplitude equations given by Eqs. (5) and (6) with supercriticality parameter $\epsilon = \frac{\sqrt{2}a_0 s\tilde{\beta}^2}{27 a_{nl}\sqrt{D_\rho}}$ and nonlinear couplings $\zeta = \frac{d_o}{2}$ and $\gamma = 2$.

Code availability. Code used to generate the data shown here are available upon reasonable request from the corresponding author.

Data availability

Data that supports the findings of this study are available upon reasonable request from the corresponding author.

Received: 29 May 2018 Accepted: 10 October 2018
Published online: 05 November 2018

References

1. Abercrombie, M. The crawling movement of metazoan cells. *Proc. R. Soc. Lond. B* **207**, 129–147 (1980).
2. Carlier, M. F. & Pantaloni, D. Control of actin assembly dynamics in cell motility. *J. Biol. Chem.* **282**, 23005–23009 (2007).
3. Blanchoin, L., Boujemaa-Paterski, R., Sykes, C. & Plastino, J. Actin dynamics, architecture, and mechanics in cell motility. *Physiol. Rev.* **94**, 235–263 (2014).
4. Schwarz, U. S. & Safran, S. A. Physics of adherent cells. *Rev. Mod. Phys.* **85**, 1327 (2013).
5. Ryan, G. L., Watanabe, N. & Vavylonis, D. A review of models of fluctuating protrusion and retraction patterns at the leading edge of motile cells. *Cytoskeleton* **69**, 195 (2012).
6. Allard, J. & Mogilner, A. Traveling waves in actin dynamics and cell motility. *Curr. Opin. Cell Biol.* **25**, 107 (2013).
7. Dreher, A., Aranson, I. S. & Kruse, K. Spiral actin-polymerization waves can generate amoeboidal cell crawling. *New J. Phys.* **16**, 055007 (2014).
8. Giannone, G. et al. Periodic lamellipodial contractions correlate with rearward actin waves. *Cell* **116**, 431 (2004).
9. Dubin-Thaler, B. J. et al. Quantification of cell edge velocities and traction forces reveals distinct motility modules during cell spreading. *PLoS ONE* **3**, e3735 (2008).
10. Döbereiner, H.-G. et al. Lateral membrane waves constitute a universal dynamic pattern of motile cells. *Phys. Rev. Lett.* **97**, 038102 (2006).
11. Ryan, G. L., Petroccia, H. M., Watanabe, N. & Vavylonis, D. Excitable actin dynamics in lamellipodial protrusion and retraction. *Biophys. J.* **102**, 1493 (2012).
12. Machacek, M. et al. Coordination of rho gtpase activities during cell protrusion. *Nature* **461**, 99 (2009).
13. Pontes, B. et al. Membrane tension controls adhesion positioning at the leading edge of cells. *J. Cell Biol.* **216**, 2959 (2017).
14. Driscoll, M. K. et al. Cell shape dynamics: from waves to migration. *PLoS Comput. Biol.* **8**, e1002392 (2012).
15. Barnhart, E. L., Lee, K.-C., Keren, K., Mogilner, A. & Theriot, J. A. An adhesion-dependent switch between mechanisms that determine motile cell shape. *PLoS Biol.* **9**, e1001059 (2011).
16. Barnhart, E. L., Allard, J., Lou, S. S., Theriot, J. A. & Mogilner, A. Adhesion-dependent wave generation in crawling cells. *Curr. Biol.* **27**, 27 (2017).
17. Yam, P. T. et al. Actin-myosin network reorganisation breaks symmetry at the cell rear to spontaneously initiate polarized cell motility. *J. Cell Biol.* **178**, 1207 (2007).
18. Lieber, A. D., Yehudai-Resheff, S., Barnhart, E. L., Theriot, J. A. & Keren, K. Membrane tension in rapidly moving cells is determined by cytoskeletal forces. *Curr. Biol.* **23**, 1409–1417 (2013).
19. Lou, S. S., Diz-Muñoz, A., Weiner, O. D., Fletcher, D. A. & Theriot, J. A. Myosin light chain kinase regulates cell polarization independently of membrane tension or rho kinase. *J. Cell Biol.* **209**, 275–288 (2015).
20. Raynaud, F. et al. Minimal model for spontaneous cell polarization and edge activity in oscillating, rotating and migrating cells. *Nat. Phys.* **12**, 367–373 (2016).
21. Gerisch, G. et al. Mobile actin clusters and traveling waves in cells recovering from actin depolymerization. *Biophys. J.* **87**, 3493 (2004).
22. Weiner, O. D., Marganski, W. A., Wu, L. F., Altschuler, S. J. & Kirschner, M. W. An actin-based wave generator organizes cell motility. *PLoS Biol.* **5**, e221 (2007).
23. Doubrovinski, K. & Kruse, K. Cytoskeletal waves in the absence of molecular motors. *EPL* **83**, 18003 (2008).
24. Shao, D., Rappel, W. J. & Levine, H. Computational model for cell morphodynamics. *Phys. Rev. Lett.* **105**, 108104 (2010).
25. Shao, D., Levine, H. & Rappel, W.-J. Coupling actin flow, adhesion, and morphology in a computational cell motility model. *Proc. Natl. Acad. Sci. USA* **109**, 6851 (2012).
26. Camley, B. A. et al. Polarity mechanisms such as contact inhibition of locomotion regulate persistent rotational motion of mammalian cells on micropatterns. *Proc. Natl Acad. Sci. USA* **111**, 14770 (2014).
27. Ziebert, F., Swaminathan, S. & Aranson, I. S. Model for self-polarization and motility of keratocyte fragments. *J. R. Soc. Interface* **9**, 1084 (2012).
28. Ziebert, F. & Aranson, I. S. Effects of adhesion dynamics and substrate compliance on the shape and motility of crawling cells. *PLoS ONE* **8**, e64511 (2013).
29. Löber, J., Ziebert, F. & Aranson, I. S. Modeling crawling cell movement on soft engineered substrates. *Soft Matter* **10**, 1365–1373 (2014).
30. Ziebert, F. & Aranson, I. S. Modular approach for modeling cell motility. *Eur. Phys. J. Spec. Top.* **223**, 1265–1277 (2014).
31. Winkler, B., Aranson, I. S. & Ziebert, F. Membrane tension feedback on shape and motility of eukaryotic cells. *Phys. D* **318-319**, 26–33 (2016).
32. Yamamoto, R., Molina, J. J. & Schnyder, S. K. Modeling of cells which migrate and proliferate on a substrate. *J. Comp. Chem. Jpn.* **17**, 14 (2018).
33. Molina, J. J. & Yamamoto, R. Mechanosensitivity of crawling cells under periodically stretching substrates. arXiv:1807.02295 (2018).
34. Najem, S. & Grant, M. Phase-field model for collective cell migration. *Phys. Rev. E* **93**, 052405 (2016).
35. Ziebert, F. & Aranson, I. S. Computational approaches to substrate-based cell motility. *npj Comput. Mater.* **2**, 16019 (2016).
36. Ziebert, F., Löber, J. & Aranson, I. S. in *Physical Models of Cell motility* (ed. Aranson, I. S.) 1–67 (Springer, Switzerland, 2016).
37. Keber, F. C. et al. Topology and dynamics of active nematic vesicles. *Science* **345**, 1135–1139 (2014).
38. Maass, C. C., Krüger, C., Herminghaus, S. & Bahr, C. Swimming droplets. *Annu. Rev. Cond. Matter Phys.* **7**, 171–193 (2016).
39. Berlyand, L., Potomkin, M. & Rybalko, V. Phase-field model of cell motility: traveling waves and sharp interface limit. *C. R. Math.* **354**, 986–992 (2016).
40. Kolmogorov, A., Petrovsky, I. & Piskunov, N. Investigation of a diffusion equation connected to the growth of materials, and application to a problem in biology. *Bull. Univ. Moscow Ser. Int. Sec. A* **1**, 1–25 (1937).
41. Aranson, I., Kramer, L. & Weber, A. Core instability and spatiotemporal intermittency of spiral waves in oscillatory media. *Phys. Rev. Lett.* **72**, 2316 (1994).
42. Marth, W. & Voigt, A. Signaling networks and cell motility: a computational approach using a phase field description. *J. Math. Biol.* **69**, 91–112 (2014).
43. Cirit, M. et al. Stochastic model of integrin-mediated signaling and adhesion dynamics at the leading edges of migrating cells. *PLoS Comput. Biol.* **6**, e1000688 (2010).
44. Murray, J. D. *Mathematical Biology. I. An Introduction* 3rd edn (Springer, Berlin, Heidelberg, 2002).
45. Fialho, A. R., Blow, M. L. & Marenduzzo, D. Anchoring-driven spontaneous rotations in active gel droplets. *Soft Matter* **13**, 5933 (2017).
46. Fujinami, N. Studies on the mechanism of circus movement in dissociated embryonic cells of a teleost, oryzias latipes: fine-structural observations. *J. Cell Sci.* **22**, 133 (1976).
47. Charras, G. T. A short history of blebbing. *J. Microsc.* **231**, 466 (2008).

48. Radszuweit, M., Engel, H. & Bär, M. An active poroelastic model for mechanochemical patterns in protoplasmic droplets of *Physarum polycephalum*. *PLoS ONE* **9**, e99220 (2014).
49. Kulawiak, D. A., Löber, J., Bär, M. & Engel, H. Oscillatory motion of a droplet in an active poroelastic two-phase model. arXiv:1803.00337 (2018).
50. Cross, M. & Greenside, H. *Pattern Formation and Dynamics in Nonequilibrium Systems*. (Cambridge University Press, Cambridge, 2009).

Acknowledgements

The work of C.R. was supported by the National Science Foundation Graduate Research Fellowship Program under Grant No. DGE-1324585. Any opinions, findings, and conclusions or recommendations expressed in this material are those of the author(s) and do not necessarily reflect the views of the National Science Foundation. B.W. and F.Z. acknowledge funding from the German Science Foundation (DFG) via project ZI 1232/2-2. I.S.A. was supported by the US Department of Energy, Office of Basic Energy Sciences, Division of Materials Science and Engineering.

Author contributions

All the authors were involved in developing the model and the numerical code. C.R. analyzed the computational modeling and performed the analytical reductions. F.Z. and I.S.A. designed and supervised the research. All authors wrote the paper.

Additional information

Supplementary Information accompanies this paper at https://doi.org/10.1038/s42005-018-0075-7.

Competing interests: The authors declare no competing interests.